

Frequency, splitting, linewidth and amplitude estimates of low- ℓ p modes of α Cen A: analysis of WIRE photometry

S. T. Fletcher^{1*}, W. J. Chaplin¹, Y. Elsworth¹, J. Schou² and D. Buzasi³

¹*School of Physics and Astronomy, University of Birmingham, Edgbaston, Birmingham, B15 2TT, UK*

²*Stanford University, HEPL Annex 201, Stanford, CA 94305-4085, USA*

³*Department of Physics, US Air Force Academy, Colorado Springs, CO 80840, USA*

12 September 2018

ABSTRACT

We present results of fitting the 50-day time series of photometry of α Cen A taken by the WIRE satellite in 1999. Both power spectrum and autocovariance function (ACF) fitting techniques were used in an attempt to determine mode frequencies, rotational splittings, lifetimes and amplitudes of low- ℓ p-modes. In all, using both techniques, we managed to fit 18 modes (seven $\ell = 0$, eight $\ell = 1$ and three $\ell = 2$) with frequencies determined to within 1 - 2 μHz . These estimates are shown to be $0.6 \pm 0.3 \mu\text{Hz}$ lower, on average, than the frequencies determined from two other more recent studies (Bouchy & Carrier 2002; Bedding et al. 2004), which used data gathered about 19 months after the WIRE observations. This could be indicative of an activity cycle, although due to the large uncertainty, more data would be needed to confirm this.

Over a range of 1700 to 2650 μHz we were also able to use the ACF fitting to determine an average lifetime of 3.9 ± 1.4 days, and an average rotational splitting of $0.54 \pm 0.22 \mu\text{Hz}$, which is the first ever reliable estimate of this parameter. In contrast to the ACF, the power spectrum fitting was shown to return significantly biased results for these parameters.

Key words: stars: oscillations – methods: data analysis

1 INTRODUCTION

The past ten years have seen a number of increasingly successful attempts to detect and measure solar-like oscillations in other stars. Due to its proximity and similarity to the Sun, many of these studies have been focused on the star α Cen A. The first clear detection of p-mode oscillations on this star was made by Schou & Buzasi (2001) from photometry using the Wide-Field Infrared Explorer (WIRE) satellite taken over a 50-day period. Schou & Buzasi (2001) correctly determined the large frequency separation but, unfortunately, wrong ℓ identifications were made and hence an incorrect value for the small separation was determined. Further detections and the first correct mode identifications were made by Bouchy & Carrier (2002) using a 13-day run of velocity measurements taken by the CORALIE spectrograph. More recently, Bedding et al. (2004) determined the frequencies for over 40 individual modes from observations by the UVES and UCLES instruments taken over a period of 5 nights.

The main driving force behind each subsequent study has been to improve the signal-to-noise ratio (SNR) in or-

der to initially detect as many modes as possible and then to better constrain the limits placed on the determined frequencies. It is of course also important to improve resolution, but practical constraints have meant all these studies were limited in the length of observations that could be made. This has meant accurate determination of mode parameters such as power, rotational splitting and lifetime has been difficult.

Here, we apply two sophisticated fitting procedures to the WIRE α Cen A data collected in 1999 in order to improve the parameter determinations. Although this data set has the poorest SNR of the three studies mentioned above, it does have the longest time series. Hence, we would expect to extract more reliable estimates of the average lifetime and rotational splitting of the α Cen A modes.

The first fitting procedure we applied was a traditional power spectrum fitting method. This involved taking the Fourier transform of the time series and then fitting a Lorentzian-like model to the various mode peaks in the resulting power spectrum. The second procedure used is a new technique based on fitting the autocovariance function (ACF) of the time series (i.e., the unnormalized autocorrelation function). Since the modes seen in the ACF are all

* E-mail: stfletch@bison.ph.bham.ac.uk

superimposed, one must first filter the time series in order to isolate the modes one is hoping to fit. The ACF can then be computed and a model based on an exponentially decaying, periodic function fitted to the result. This technique was first introduced as a possible method for mode determination by Gabriel et al. (1998) and developed more fully by Fletcher, Chaplin & Elsworth (2004) in an attempt to better constrain mode parameters of long solar p-mode data sets.

In the initial investigation of the WIRE data by Schou & Buzasi (2001) only a handful of modes were identified due to the poor SNR in the data set. However, a distinct advantage of revisiting this data comes in having a large number of robust mode identifications from the aforementioned two later studies. This provides additional a-priori information that we can use as initial ‘guess’ values for our fitting procedures.

In order to fully test our fitting of the WIRE data we also generated a set of artificial time series. These data were created specifically to mimic the WIRE data allowing us to explicitly determine the precision and robustness of our fitted parameters. We detail the creation of this simulated data in Section 2. In Section 3 we describe in detail the procedure involved in applying the two fitting techniques to the data. Finally, in Section 4, we go on to present and analyse the results of our fitting for the mode frequencies, amplitudes, lifetimes and rotational splitting parameters.

2 DATA

The WIRE satellite collected 50 days of photometry observations on the star α Cen A between July 15 and September 3, 1999. The orbit was 96 minutes, low Earth and Sun-synchronous, which unfortunately lead to rather significant pointing constraints. Hence, observations could only be made for about 40 minutes out of each orbit. Additionally there were some days when no data were collected and some days where data could not be used due to processing problems. Hence, the resulting duty cycle for the WIRE time series was only 15%. The processing of the WIRE data to produce the final time series is described in Buzasi et al. (2000) and Schou & Buzasi (2001). The data were binned to a 10s cadence resulting in a series of 432,000 points. The processed time series is shown in Fig 1, for both the full 50 days and a zoomed in section with just the first 8 days in order to show the main gap structure. Being as the time series was made using photometry observations, the amplitudes are given in parts-per-million (ppm). The method for converting between ppm and velocity is described in Section 4.5.

A full set of simulated data made to resemble the WIRE time series was produced in order to test fitting on the real data. The Laplace transform solution of the equation of a forced, damped harmonic oscillator was used in order to generate individual mode components of the artificial time series. The application of this model is described more fully in Chaplin et al. (1997). A set of low- ℓ modes covering the ranges $0 \leq \ell \leq 2$ and $1700 \leq \nu \leq 2650 \mu\text{Hz}$ was created in this way. It should be noted that the $\ell = 3$ modes are not included since they do not appear to be detectable in the WIRE photometry data, although for more

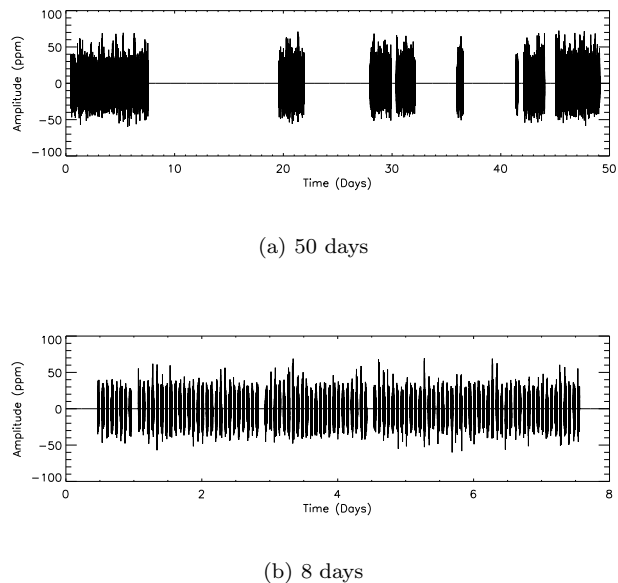


Figure 1. The Wire α Cen A time series over (a) the full 50 days and (b) the first 8 days only.

recent velocity observations they are (Bedding et al. 2004). For each $\ell \neq 0$, a rotationally induced splitting pattern was included, for which the visibilities, ε , of each component were fixed using the following equations (Gizon & Solanki 2003; Toutain & Gouttebroze 1993)

$$\varepsilon_{1,0} = \cos^2 i, \quad (1)$$

$$\varepsilon_{1,\pm 1} = \frac{1}{2} \sin^2 i, \quad (2)$$

$$\varepsilon_{2,0} = \frac{1}{4} (3 \cos^2 i - 1)^2, \quad (3)$$

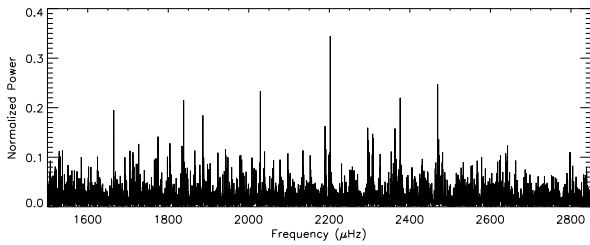
$$\varepsilon_{2,\pm 1} = \frac{3}{8} \sin^2(2i), \quad (4)$$

$$\varepsilon_{2,\pm 2} = \frac{3}{8} \sin^4 i, \quad (5)$$

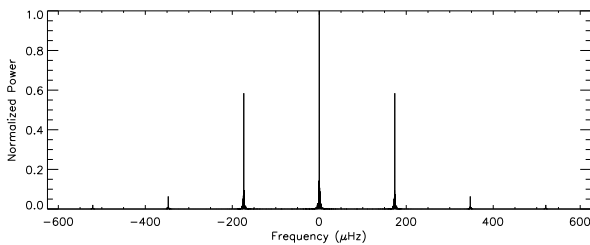
and the inclination, i , was chosen as 79° (Pourbaix, Neuforge-Verheecke & Noels 1999).

A database of frequency and powers, based on preliminary fits to the WIRE data, was used in order to fix the various characteristics of each mode. Where no modes could be identified, frequencies presented in Bedding et al. (2004) were used.

Based on fits to the ACF of the WIRE data (see section 3.2) we chose a constant rotational splitting of $0.5 \mu\text{Hz}$ and a constant linewidth (full width half maximum) of $1.0 \mu\text{Hz}$ (equivalent to a lifetime or e-folding amplitude time of ~ 3.7 days). Analysis of fits to these artificial data (see sections 4.2 and 4.3) showed the parameters could be robustly determined. This gives confidence that the simulated spectra were a good match to, and a reliable cross check for, the real data. A background offset (white noise) was also added so as to match the WIRE data. In total 50 independent data sets were created, each of a length equal to the WIRE time series. The WIRE window function was imposed on each of them.



(a) The WIRE Power Spectrum



(b) The WIRE Spectral Window

Figure 2. A (a) The WIRE Power Spectrum over the region $1500 \leq \nu \leq 2850 \mu\text{Hz}$ and (b) the spectral window plotted over the same total frequency range.

3 MODELLING AND FITTING

In this section we outline the two different methods used to determine the various p mode parameters. First we discuss the more traditional power spectrum technique and then go onto introduce the ACF method. In both cases we explain the specific models used to fit the WIRE data.

3.1 Power Spectrum

When fitting the power spectrum of a solar or solar-like p -mode time series the various mode components are generally modelled using either a Lorentzian, or an asymmetric function that models small departures from a symmetric shape (Nigam & Kosovichev 1998). For low- ℓ (Sun-as-a-star) data this is commonly done by fitting individual mode pairs (i.e., $\ell = 0$ with neighboring $\ell = 2$; and $\ell = 1$ with $\ell = 3$) using narrow fitting ‘windows’ centered on the target pair.

Unfortunately, certain characteristics of the WIRE data make this strategy difficult to implement. The rather severe window function mentioned in Section 2 results in prominent sidebands at $173.6 \mu\text{Hz}$ from the mode peaks. As a result the sidebands of modes lie in the vicinity of other overtones. This makes it very difficult to isolate a single mode pair and its sidebands without the presence of intervening modes. Therefore, we adopt a strategy of fitting Lorentzian profiles to all modes simultaneously. Note that the WIRE power spectrum and the spectral window are shown in Fig. 2

In the $1700 \leq \nu \leq 2650 \mu\text{Hz}$ range a total of 27 modes were included in the simulated data sets: 9 each of $\ell = 0, 1$ and 2. The $\ell = 1$ and 2 modes were split into three and five

Table 1. n and ℓ values included in fitting.

n	ℓ	n	ℓ
14	2	19	0,1
15	1	20	0,1
16	0,1	21	0,1,2
17	0,1,2	22	0
18	1	23	0,1

components respectively to match the rotational splitting pattern. However, we chose to fit only the modes that are identifiable in the WIRE data, of which there are eighteen.

For the power spectrum method, the power spectral density, P , was modelled using a standard Lorentzian profile for each peak summed over all visible modes and corresponding sidebands in the chosen frequency range, offset with a flat background, B , i.e.,

$$P = B + \sum_{nlmk} H_{nlmk} Z_{nlmk}^{-1}, \quad (6)$$

where

$$Z_{nlmk} = 1 + \left(\frac{\nu - \nu_{nl} + ms + kw}{\Delta/2} \right)^2.$$

Here, H is the height of each mode component (i.e., maximum power spectral density), ν_{nl} is the central frequency of a mode, s is the rotational splitting, w is the sideband spacing and Δ is the width.

In the WIRE data, over the range $1700 \leq \nu \leq 2650 \mu\text{Hz}$, the radial overtone number, n , increases from 14 to 23. However, since we fit only 18 modes we do not sum over all the possible $n\ell$ combinations. Table 1 gives the list of n and ℓ -valued modes that are fitted. m is the azimuthal order and is summed over $-\ell \leq m \leq \ell$, while k is a dummy variable allowing us to include the first order sidebands in our model and as such is summed over $-1 \leq k \leq 1$.

Sidebands were assumed to lie at a fixed spacing of $173.6 \mu\text{Hz}$ and to have the same width as the main peaks. The fractional height of the sidebands were also fixed according to the ratio of the sidebands to the main peak in the Fourier transform of the window function. In this way, we did not fit any parameters associated solely with the sidebands.

The number of fitted parameters was further reduced by assuming fixed height ratios for the rotationally split components. These were fixed according to equations 1 to 5, again assuming an inclination for α Cen A of 79° .

Finally, it should be noted that because of the relatively short duration of the time series and the poor SNR, we did not feel that the data justified the use of the more complicated asymmetric Nigam & Kosovichev (1998) model.

To fit the model to the power spectrum we used a Powell multi-dimensional hill-climbing minimization algorithm, which maximized an appropriate log-likelihood function. This function was based on the assumption that the power spectrum is distributed with negative exponential (i.e., χ^2 , with two degrees of freedom) statistics. The following parameters were varied iteratively until they converged on their best fitting values.

- (i) A frequency for each mode.

(ii) A single height for each mode. Heights of rotationally split components were fixed relative to the strongest outer $\ell = |m|$ components (see equations 1 to 5).

(iii) A single width for all modes.

(iv) A single splitting for the $\ell = 1$ and 2 modes

(v) A flat, background offset for the whole fit.

A total of $2M+3$ parameters were therefore fitted where M is the number of modes included in the fitting (i.e., 18 in this case). We should add that in order to recover the power, (i.e., the square of the amplitude), A^2 , in each mode from the fitted height, H , and the width, Δ , we used the following expression:

$$A^2 = H \left(\frac{\pi}{2} T \Delta + 1 \right), \quad (7)$$

where T is the length of the time series. Details on the derivation of this expression are given in the appendix.

3.2 The Auto-Covariance Function

The Autocovariance Function (ACF) is the product of a data series with a shifted versions of itself over successive time lags, τ . For a time series of discrete measurements, x_i , it is defined as:

$$Y_\tau = \frac{\sum_{i=0}^{(N-1)-\tau} (x_i - \bar{x})(x_{i+\tau} - \bar{x})}{N - \tau}. \quad (8)$$

where N is the number of points in the data series and \bar{x} is the mean of the sample. In many data series the mean is often very close to zero, as is the case for p-mode intensity or Doppler velocity residuals, in which case the ACF reduces to:

$$Y_\tau = \frac{\sum_{i=0}^{(N-1)-\tau} x_i x_{i+\tau}}{N - \tau}. \quad (9)$$

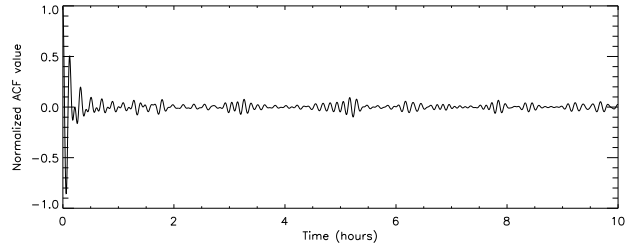
The more commonly used normalized version of the autocovariance function is termed the autocorrelation function and for a time series with zero mean is given by:

$$\rho_\tau = \frac{\sum_{i=0}^{(N-1)-\tau} x_i x_{i+\tau}}{N - \tau \sum_{i=0}^{N-1} x_i^2}. \quad (10)$$

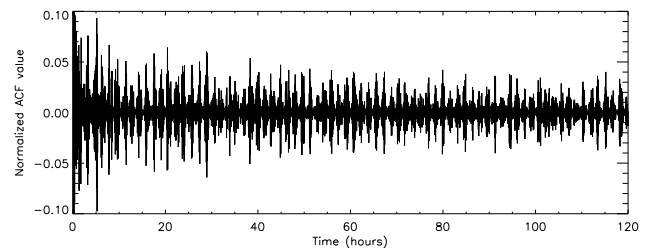
However, by fitting the autocovariance function we can directly obtain absolute estimates of the powers associated with the modes, as opposed to relative powers that would be obtained from fitting the autocorrelation function.

Since the ACF is computed in the time domain, the periodic waveforms of the various components are superimposed. Therefore, to fit a certain set of modes in a given frequency range one must first apply a band-pass filter to the time series. As the observable modes in the WIRE data lie in the region $1700 \leq \nu \leq 2650 \mu\text{Hz}$ we need to at least filter over this range. However, we must also take into account the effect of the window function. As one would expect, the sidebands in the power spectrum manifest in the ACF as additional waveforms. Hence, we choose to extend the bandpass range to $1500 \leq \nu \leq 2850 \mu\text{Hz}$ in order to include all the sideband frequencies.

In Fig. 3 we show the normalized ACF (i.e., the autocorrelation function) of the WIRE time series, filtered between $1500 \leq \nu \leq 2850 \mu\text{Hz}$, and plotted over: the first 3600 points (10 hours) in Fig. 3(a); and over the first 43200 points (120



(a) ACF – 10 hours



(b) ACF – 120 hours

Figure 3. Normalized ACF of WIRE data over (a) the first 10 hours and (b) the first 120 hours. The scale has been reduced in (b) in order to better show the features.

hours) in Fig. 3(b). The filtering was performed using a non-recursive digital filter (Walraven 1984). There are a number of distinctive features in the ACF the most striking being the very sharp decay in the ACF that occurs over the first few hours. This is due to the poor SNR in the WIRE data and is explained in more detail below.

After this initial decay the ACF structure is dominated by the p-mode signal. On the smallest timescale, there is a quasi sinusoidal waveform with a period of about 7.5 minutes. This particular feature can be seen in Fig. 3(a) but is too rapid to be seen in Fig. 3(b). It is due to the main set of modes that are seen at around $2000 \mu\text{Hz}$ in the α -Cen spectrum. On a longer timescale we see quasi-periodic structure close to ~ 1.5 hours. This is due to the prominent sidebands which occur at $173.6 \mu\text{Hz}$ to either side of the main peaks. We also see a hint of a ~ 5 -hour quasi-periodic structure due to the separation between $\ell = 0$ and $\ell = 1$ modes. Longer time scale quasi-periodic variations due to smaller mode spacings, such as those between adjacent modes in the low- ℓ pairs, and rotational splitting, are more difficult to observe and therefore extract. However, there is evidence of an overall exponential decay in the structure of the ACF due to the finite lifetimes of the modes.

The ACF was modelled using a damped harmonic oscillator equation summed over all visible modes and corresponding sidebands in the chosen frequency range with an additional background function, B_τ ,

$$f_\tau = B_\tau + \sum_{nlmk} A_{nlmk}^2 \cos(\omega_{nlmk} t_\tau) \exp(-\gamma t_\tau), \quad (11)$$

where,

$$\omega_{nlmk} = \sqrt{(2\pi(\nu_{nl} + ms + kw))^2 - \gamma^2},$$

A^2 is the mode power, ω is the natural angular frequency of the mode, γ is the damping constant and t is time. Note that γ is related to the width of mode peaks by $\Delta = \gamma/\pi$. B_τ is the background component but in the ACF this is not a simple offset but must be treated according to the expression:

$$B_\tau = b \left(\frac{\sin(2\pi\nu_1 t_\tau)}{2\pi\nu_1 t_\tau} \right) \cos(2\pi\nu_2 t_\tau),$$

where b is the power in the background and is the parameter to be fitted. ν_1 is a value given by the extent of the filtered frequency range divided by 2 (i.e., 675 μHz in this instance) and ν_2 is the central frequency in the filtered range (i.e., 2175 μHz). The sinc term is a direct result of filtering over a finite frequency range. The wider this range the higher the frequency and the faster the background function decays. It is this decay that dominates the first few time samples of the WIRE ACF. The extra waveforms due to the window function are included in the model in the same way as sidebands were treated in the power spectrum.

For the ACF, a gradient-expansion algorithm was used to perform a non-linear least-squares fit to our model, with

$$\chi^2 = \sum_{\tau} \frac{[Y_\tau - f(t_\tau, \mathbf{a})]^2}{\sigma_\tau^2} \quad (12)$$

the quantity to be minimized, where Y are the data, f is the model, t is time, \mathbf{a} is the vector of parameters and σ is the expected error on each point of the ACF. Note that we are essentially fitting the same set of parameters as with the power spectrum except the power (square of the amplitude) in the modes is fitted directly.

We note that two assumptions are made in order to simplify fitting the model to the ACF. Firstly, we take the error distribution, σ_τ to be constant over the range of the ACF that we fit. A plot of the standard deviation over all the ACF's of the simulated data shows this to be a reasonable approximation. Secondly, we ignore the effect of correlation between one point in the ACF and the next. While correlation clearly must be present, the effect of ignoring it can be shown to only affect attempted error calculations and not the fitted values themselves (Kuan 2000); hence the reason for using Monte Carlo simulations to fix the errors on our fits.

4 RESULTS AND ANALYSIS

In this section we present the results and analysis of fitting the WIRE data using the two methods described in Section 3. We initially show a graphical representation of the fitted model overlaid on the power spectrum before analyzing the four different types of parameters fitted (frequencies, linewidth, amplitudes and background) in more detail in separate subsections.

4.1 Graphical Representation of the Fits

In order to give a clear picture of the fits as determined from the power spectrum fitting technique, Fig. 4 shows the fitted

model overlaid on the WIRE power spectrum in the region $1700 \leq \nu \leq 2500$ μHz . This plot shows a very good illustration of the fitted splittings. (Note that in sections 4.3 and 4.4 we show that fits to the power spectrum have a tendency to slightly overestimate the splitting and underestimate the width.)

The fitted peaks that are not labelled in the plot are the first order sidebands. The dotted line extending outwards from the strong $n=19$, $\ell=1$ peak shows the frequency spacing at which the associated sidebands are placed. Having sidebands occur at such a large distances from their main peak is somewhat unusual for those more used to dealing with diurnal sidebands.

On closer inspection of the plot, there are some fitted modes that have very small powers (namely the $n=17$, $\ell=1$, $n=20$, $\ell=0$ and the $n=21$, $\ell=1$ modes) and as such, the reliability of these fits is somewhat questionable. The reason for their presence is that the fitting routine attempts to fit peaks for all the modes included in the model. Hence, if a mode is expected at a certain frequency, and there is no large and obvious peak in the nearby vicinity, the fitting routine may latch on to a smaller peak which is only associated with the background noise. However, with these fitted modes having such small powers, even if they are not true signatures of mode excitation, their effect on the overall width and rotational splitting estimates is negligible.

In Fig. 5, four 15 μHz slices of the spectrum are shown, each located on fairly strong modes. For the $\ell=1$ and $\ell=2$ modes, it is possible to identify a rotational splitting pattern in the spectrum, and the model is seen to fit reasonably well. While we would also like to be able to show similar graphical illustrations of the splitting and widths as determined from the ACF fitting, the superimposed nature of the waveforms makes this difficult.

4.2 Mode Frequencies

Both methods produced well-constrained frequency estimates for seventeen out of eighteen of the modes we tried to fit. Sixteen of these were determined via both methods while the other two modes were fitted by one method only. The fitted frequencies are shown in Tables 2 and 3 respectively where the quoted uncertainties were determined from the standard deviation of fits made to the 50 simulated spectra. The errors are quite large for some of the estimates due to the high background and resulting poor SNR of the WIRE data. A comparison between the two sets of results shows the differences to be very small. The root-mean-square (rms) difference is 0.3 μHz , compared with an average error of 1.4 μHz .

We can also compare our frequencies with those determined by Bedding et al. (2004) and Bouchy & Carrier (2002). Looking at individual modes we see differences of the order of 1 μHz which is within the errors given. However, when taking a weighted average of the differences we find the estimates from the WIRE data are about 0.8 ± 0.3 μHz lower than the frequencies determined from Bedding et al. (2004) and Bouchy & Carrier (2002). One contribution to this difference comes from the shift in the mode frequencies due to the relative motion of the Earth around its orbit. By considering the times of year during which the observations were carried out, and the ecliptic coordinates of α Cen A, it

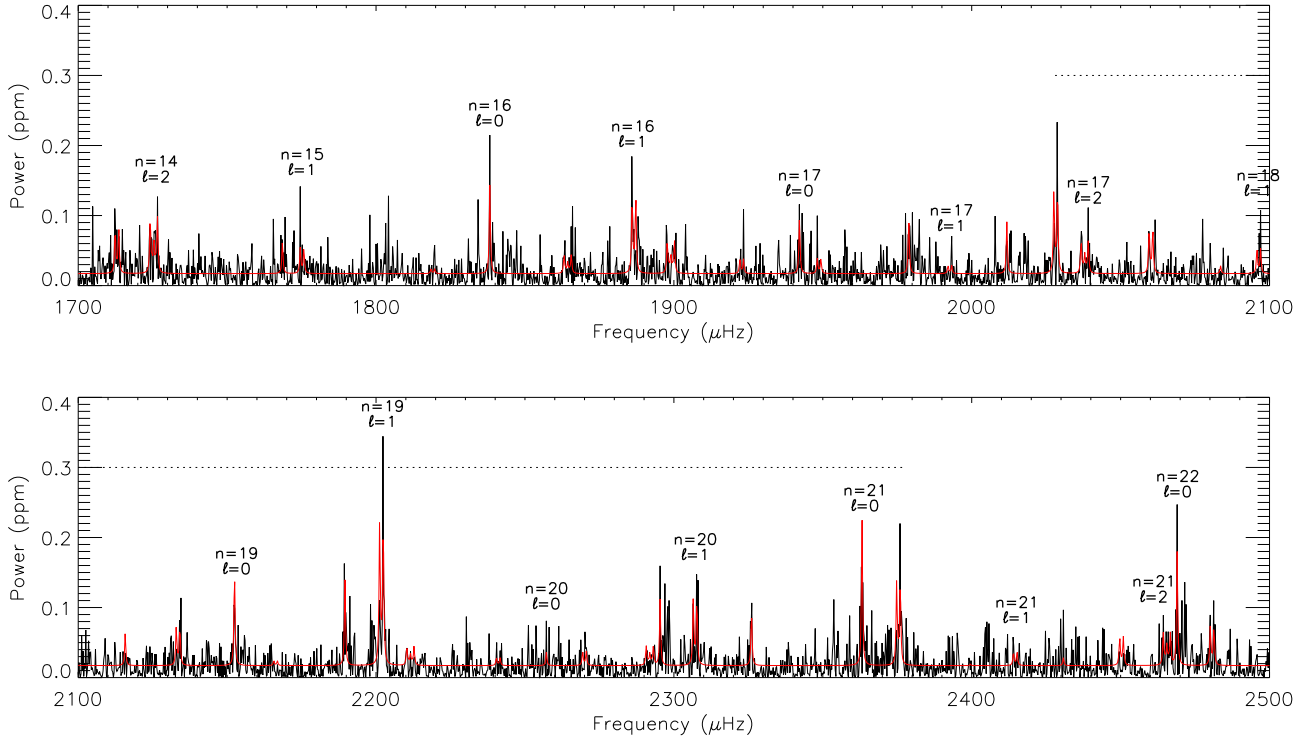


Figure 4. WIRE Spectrum for the region $1700 \leq \nu \leq 2500 \mu\text{Hz}$, with the fitted model overlaid. The fitted modes are labelled and the horizontal lines extending from the strong peak at $\sim 2200 \mu\text{Hz}$ indicate the scale of the sideband distance. Three of the modes have very questionable fits, those at $n=17, \ell=1$, $n=20, \ell=0$ and $n=21, \ell=1$.

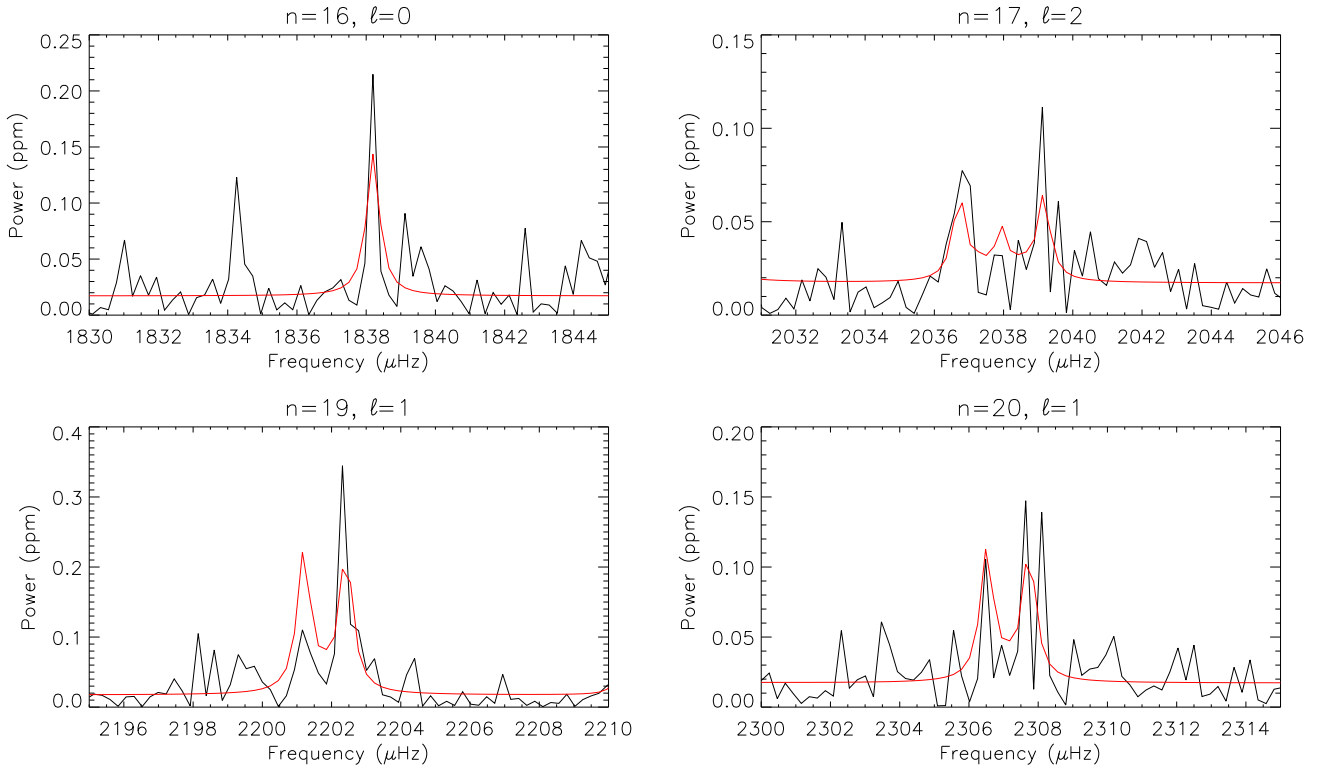


Figure 5. $15 \mu\text{Hz}$ slices of the WIRE spectrum showing the fits for four different modes.

Table 2. Frequencies extracted by power spectrum fitting method (μHz). Brackets indicate modes with questionable fits, see Section 4.1

n	$\ell=0$	$\ell=1$	$\ell=2$
14			1725.4 ± 1.5
15		1775.2 ± 1.3	
16	1838.2 ± 1.2	[1886.6 ± 1.7]	
17	1942.4 ± 1.0	1992.7 ± 1.8	2037.9 ± 1.4
18		2096.4 ± 1.6	
19	2152.5 ± 1.0	2201.8 ± 0.7	
20	[2257.2 ± 1.4]	2307.1 ± 1.2	
21	2363.2 ± 1.0	[2414.6 ± 1.4]	2465.5 ± 1.8
22	2469.0 ± 0.9		
23		2623.9 ± 1.3	

Table 3. Frequencies extracted by ACF fitting method (μHz).

n	$\ell=0$	$\ell=1$	$\ell=2$
14			1725.3 ± 1.8
15		1774.9 ± 1.5	
16	1838.5 ± 1.2	1886.6 ± 1.7	
17	1942.4 ± 1.3	[1993.1 ± 1.8]	2038.8 ± 1.9
18		[2096.9 ± 1.9]	
19	2152.5 ± 0.9	2202.1 ± 0.7	
20	[2257.1 ± 1.5]	2307.7 ± 1.1	
21	2363.4 ± 0.8		2465.6 ± 2.2
22	2469.2 ± 0.8		
23	2578.3 ± 1.7	2624.3 ± 1.4	

can be shown that this effect should lead to the WIRE data having frequencies $\sim 0.2 \mu\text{Hz}$ lower than the other two data sets. Therefore, the corrected difference is $0.6 \pm 0.3 \mu\text{Hz}$, which is only significant at 2 sigma.

Since the WIRE data set is taken 19 months prior to the others one might conjecture that the difference is due to an activity cycle on α Cen A. Were a $0.6 \mu\text{Hz}$ shift over a period of just 19 months to be real, it would suggest a large and rapid (or possibly just very large) activity cycle. By comparison, the minimum to maximum change in mode frequencies due to the solar cycle, is $\sim 0.4 \mu\text{Hz}$ and this occurs over a 5.5-year period. Of course, a zero or very small shift is not ruled out and so it is clear that further and better quality sets of observations would be needed in order to make any solid conclusions.

As well as using the simulated data to estimate the uncertainties on our fits we also used them to test accuracy and reliability. The plots in Fig. 6 show the mean difference between the fitted and input frequencies of the simulations. The associated error bars are the error on the mean, given by the standard deviation divided by the square root of the number of fits. For both methods the estimates are generally accurate to within errors and there does not seem to be any particular bias towards an under or overestimation of the input frequency.

The errors on the real data estimates given in Tables 2 and 3 and on the artificial data estimates in Fig. 6 show how the uncertainties vary quite substantially from one mode to the next. This is to be expected since the uncertainties

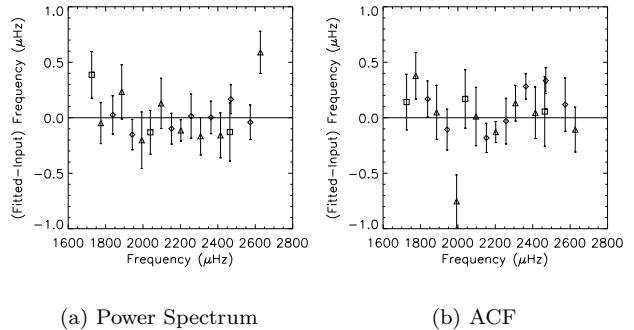


Figure 6. Results of fitting artificial WIRE-like data. Average difference between fitted and input frequencies for $\ell=0$ (diamonds), $\ell=1$ (triangles) and $\ell=2$ (squares) modes. Error bars indicate the error on the mean as given by the standard deviation in the fitted frequencies divided by the square root of the number of fits.

depend strongly on the SNR, when the SNR is poor. The equation (Libbrecht 1992; Toutain & Appourchaux 1994):

$$\sigma_{v_{nl}}^2 = \frac{\Delta}{4\pi T} \sqrt{\beta+1} (\sqrt{\beta+1} + \sqrt{\beta})^3, \quad (13)$$

gives an estimate of the error on the fitted frequency, $\sigma_{v_{nl}}$ as a function of the linewidth, Δ , the length of the time series, T and the noise-to-signal ratio, β (i.e the inverse of the SNR). When the SNR is high, β is small, and the level of uncertainty will be dominated by Δ and T and as such will remain fairly constant from mode to mode. However, for a poor SNR, the β term is important and so small changes in this, due to the difference in amplitudes of the modes, will have a large effect on the uncertainty.

The relationship between the SNR and the errors on the frequencies can be seen more clearly by plotting the standard deviation against the input amplitude of the modes, as in Fig. 7 (this is equivalent to plotting against the signal-to-noise in amplitude since the background is kept constant with frequency). The large SNR in the WIRE data also means that the typical uncertainties on our frequency estimates are somewhat larger than those given by Bedding et al. (2004), which were $\sim 0.3 \mu\text{Hz}$.

4.3 Rotational Splitting

There have to date been no successful attempts to measure the rotational splitting of the p -modes in α Cen A and thereby make a first step to constraining the internal rotation. However, by applying the ACF fitting technique to the WIRE data and assuming a constant splitting across the frequency range we have been able to determine a reasonably well constrained estimate of $0.54 \pm 0.22 \mu\text{Hz}$. The simulated data were again used in order to check the accuracy of this estimate. By fitting the ACF of the 50 artificial data sets an average splitting of $0.44 \pm 0.03 \mu\text{Hz}$ was returned. This was within 2 standard errors of the input value of $0.5 \mu\text{Hz}$, indicating that the fits are relatively unbiased. It should be noted that of the 50 estimates returned via the ACF method, 10 gave a splitting very close to zero. These ‘null’ splitting results are a common problem when fitting

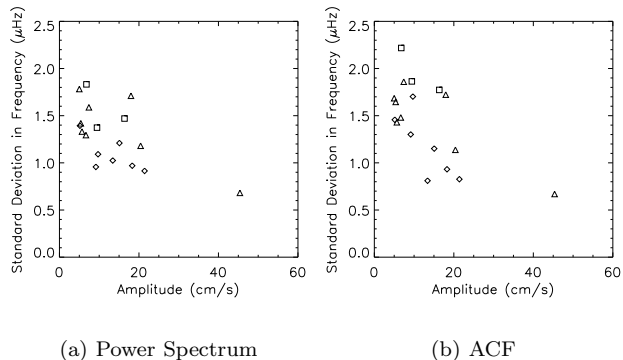


Figure 7. Results of fitting artificial WIRE-like data. Standard deviation of fitted frequencies as a function of the input amplitude of the modes. Symbols have the same meanings as in Fig. 6.

poorly defined modes (either due to poor resolution, low SNR or a large width-to-splitting ratio), and we have taken the usual step of disregarding these values when determining the mean and standard deviation of the fits to the simulated data (Chaplin et al. 2001).

A value of the splitting was also returned when fitting the power spectrum. This method gave an estimate of $0.64 \pm 0.25 \mu\text{Hz}$, which is within errors of the estimate given by fitting the ACF. However, fits to the simulated data showed a tendency for the estimates of the splitting to overestimate the true input value. An average of 0.68 ± 0.03 was returned which gives a result which is ~ 6 standard errors too large. This is also a common problem in the solar case but is generally due to a large width-to-splitting ratio at high frequencies rather than a poor SNR. Because of the bias in the power spectrum estimate we would suggest that the value of the rotational splitting returned via fitting the ACF is more robust.

A rotational splitting of $0.54 \pm 0.22 \mu\text{Hz}$ gives a rotational period of 21_{-5}^{+17} days. This agrees with a measurement of the α Cen A surface rotation rate determined by Jay et al. (1996) of 23_{-2}^{+5} days using chromospheric and transition region emission line features as markers of rotation. Also, a surface rotation rate of $2700 \pm 700 \text{ ms}^{-1}$ from Saar & Osten (1997) coupled with theoretical predictions of the alpha Cen A radius of $1.23 R_{\odot}$ (Morel et al. 2000), give a prediction of 23 ± 6 days. A similar correspondence of the low- ℓ splittings and the surface rate of rotation is seen for the Sun.

4.4 Linewidths and Lifetime

Since our model also assumed a fixed value for the linewidth we were able to obtain a well constrained estimate of this parameter. However we lose any knowledge of how the parameter varies with frequency. Our estimate for the average linewidth of the modes from fitting the ACF of the WIRE time series is $0.92 \pm 0.30 \mu\text{Hz}$, which equates to a lifetime of 3.9 ± 1.4 days. Fits to the ACF of the simulated data gave an average width of $1.10 \pm 0.05 \mu\text{Hz}$, which is again within 2 standard errors of the input value of $1.0 \mu\text{Hz}$. Our fits to the artificial data also showed a clear anti-correlation between the fitted linewidths and the fitted rotational split-

Table 4. Amplitudes extracted by power spectrum fitting method (cms^{-1}). Brackets indicate modes with questionable fits.

n	$\ell=0$	$\ell=1$	$\ell=2$
14			41_{-14}^{+34}
15		13_{-5}^{+18}	
16	23_{-8}^{+21}	41_{-12}^{+34}	
17	14_{-5}^{+12}	$[4_{-4}^{+13}]$	23_{-9}^{+20}
18		13_{-6}^{+19}	
19	24_{-8}^{+26}	76_{-30}^{+54}	
20	$[3_{-4}^{+15}]$	35_{-14}^{+38}	
21	38_{-7}^{+14}	$[7_{-4}^{+17}]$	24_{-7}^{+15}
22	29_{-13}^{+34}		
23		26_{-6}^{+19}	

tings. This meant that the fits that returned ‘null’ splittings also returned artificially high linewidths, as one might expect. We therefore removed these fits from our calculation of the mean and standard deviation of the artificial results, in the same manner as for the rotational splitting.

Our estimates of the linewidth from fitting the power spectrum gave us a much smaller value of $0.46 \pm 0.38 \mu\text{Hz}$, which is a lifetime of 8.1 ± 6.8 days. However, fits to the simulated data showed estimates of the linewidth to be significantly underestimated. An average fitted value across the 50 data sets of $0.62 \pm 0.06 \mu\text{Hz}$ was returned indicating an underestimate of over 6 standard errors. The same anti-correlation between linewidth and rotational splitting values that was seen when fitting the ACF was also seen here with overestimates of the splitting being combined with underestimates in the linewidth. This leads us to conclude that the ACF fitting technique also gives a more reliable estimate of the linewidth and hence lifetime of the α Cen A p-modes.

In relation to our assumption that fitting a constant width returns the average linewidth across the fitted modes we note that the ACF fitting has also been tested on artificial data simulating solar oscillations, for which the linewidth varies with frequency. In this case we found that fitting a constant width did indeed return the input average across the modes.

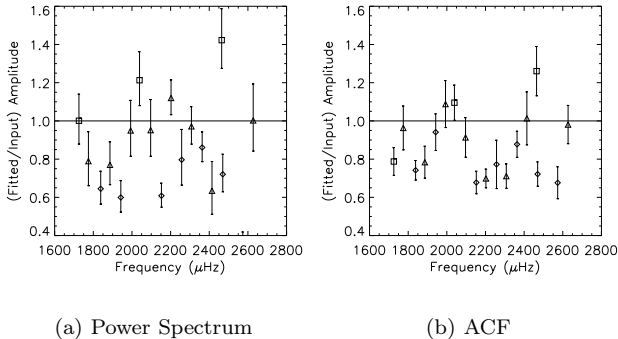
The Bouchy & Carrier (2002) and Bedding et al. (2004) studies were both made from observations lasting just a few days (5 and 12 respectively) and a direct measurement of the mode lifetime was difficult to achieve. However, Bedding et al. (2004) were able to develop a method of estimating the lifetime from the scatter in the frequency measurements. Their initial estimate put the average mode lifetime at $1.4_{-0.4}^{+0.5}$ days at 2.1 mHz, however, that has recently been reevaluated as $2.3_{-0.6}^{+1.0}$ days (Kjeldsen et al. 2005). This estimate is smaller than our value determined from fitting the ACF of the WIRE data, although the error bars overlap.

4.5 Mode Amplitudes

We have chosen to present the strength of the modes in terms of their amplitudes rather than power. We have also converted the units to velocity (cms^{-1}) even though the WIRE observations were intensity measurements. In both cases this was done so as to more easily make comparisons

Table 5. Amplitudes extracted by ACV fitting method (cm s^{-1}).

n	$\ell=0$	$\ell=1$	$\ell=2$
14			25 ± 12
15		12 ± 7	
16	24 ± 8	25 ± 16	
17	17 ± 9	[4 ± 7]	19 ± 9
18		[6 ± 8]	
19	24 ± 10	52 ± 20	
20	[4 ± 7]	22 ± 13	
21	29 ± 8		17 ± 8
22	23 ± 14		
23	13 ± 8	19 ± 6	


Figure 8. Results of fitting artificial WIRE-like data. Average ratios of fitted to input amplitudes. Symbols have the same meaning as in Fig. 6.

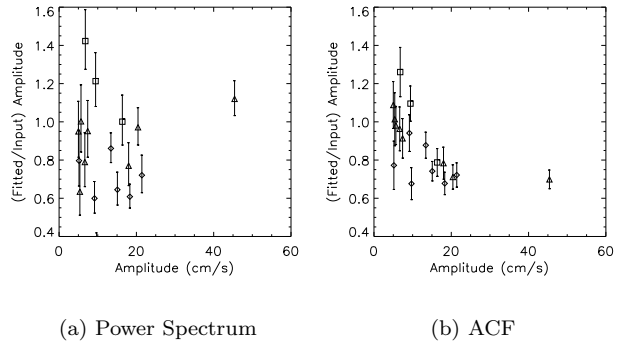
with the Bedding et al. (2004) study. To convert between intensity given in parts per million (ppm) and velocity we use the expression given in Kjeldsen & Bedding (1995):

$$v_{\text{osc}} = \left(\frac{\delta L}{L} \right)_{\lambda} \left(\frac{\delta L}{550\text{nm}} \right) \left(\frac{T_{\text{eff}}}{5777\text{K}} \right)^2 \left(\frac{1}{20.1\text{ppm}} \right) \quad (14)$$

where v_{osc} denotes the amplitude of velocity oscillations in ms^{-1} , $(\delta L/L)_{\lambda}$ the change in intensity at the effective wavelength λ ($\sim 450\text{nm}$ for WIRE), T_{eff} the effective temperature of the star (~ 5770 for α Cen A) and 5777K is taken as the effective temperature of the Sun.

Of the four types of parameter examined in this paper the amplitudes are the least well constrained. This is because we have attempted to fit a separate power to each mode, rather than an average value across several modes as was done with the linewidth and splitting. This results in large uncertainties on the amplitude estimates as shown in Tables 4 and 5 for the power spectrum and ACF fitting respectively. Indeed the errors on some of the weaker modes are larger than the actual estimated powers. Hence, we cannot put much credence in these values as they will be dominated by background noise.

We have again used simulated data to test the accuracy of the fitted powers. In a similar fashion to that used for the fitted frequencies, we have plotted in Fig. 8 the difference between the power estimates averaged over the 50 artificial data sets and the input values. The plots show that both methods return a number of estimates that sig-


Figure 9. Results of fitting artificial WIRE-like data. Average ratios of fitted to input amplitudes, plotted as a function of input amplitude. Symbols have the same meaning as in Fig. 6.

nificantly underestimate the true input amplitude. In Fig. 9 we plot the same data but as a function of the mode amplitude. This shows that when fitting the ACF, the amplitude of the stronger modes seem to be underestimated by around 30 percent, whereas the weaker modes suffer less bias. This pattern is less obvious when fitting the power spectrum with little evidence of the bias being dependent on the strength of the modes. Fig. 8, also shows a tendency for the power of the lower ℓ -valued modes to underestimate the input values more so than for higher ℓ -valued modes. This is particularly noticeable for the power spectrum fits.

5 SUMMARY

The 50-day time series of photometry observations taken in 1999 by the WIRE spacecraft has been reanalysed using power spectrum and autocovariance fitting methods. With the help of a-priori information, regarding the location in frequency of modes from other recent α Cen A studies, we have managed to fit 18 different modes in the power spectrum and autocovariance function (ACF), 16 of which were fitted in both. The values of the fitted frequencies are slightly lower than those determined by Bedding et al. 2004 and Bouchy & Carrier 2002, although without better data we cannot say with any confidence whether this is indicative of an activity cycle for α Cen A.

In addition to the frequencies we have also been able to estimate an average rotational splitting across the fitted modes of $0.54 \pm 0.22 \mu\text{Hz}$ using the ACF. An average lifetime was also estimated by fitting the ACF and was found to be 3.9 ± 1.4 days. Although the actual fitted value is larger than the lifetime estimated by Kjeldsen et al. (2005), the error bars do overlap. Estimates of the amplitude were also obtained, however they were rather poorly constrained, especially for the weaker modes.

Simulated time series made to mimic the WIRE data were created in order to test the accuracy and precision of the fitting methods using a Monte Carlo approach. We found that for the most part, the fitted parameter estimates averaged over a number of realizations agreed with the input values used to create the data. However, we did find that fits to the power spectrum tended to underestimate the linewidths

and overestimate the splittings. The bias on both of these parameter estimates were reduced when fitting the ACF.

There still may be opportunities to refine this work further. For example, in this analysis, a fairly basic approach to dealing with the window function was employed, simply allowing for the subsequent sidebands in the models. A more sophisticated approach for fitting the power spectrum would be to convolve the spectral window with the model and fit that to the data. Also, because of the Weiner-Khinchine relation, that states that the ACF is actually the Fourier transform of the power spectrum, this technique can probably be applied to the ACF fitting approach as well. Additionally, there is now a new set of WIRE α -Cen observations that was taken in January 2004 and lasted for around 30 days. If modes can be identified and fitted from this data as well, it will give an excellent comparison with the 1999 time series and should allow for a better investigation into a possible activity cycle.

ACKNOWLEDGMENTS

We would like to thank all those who are, or have been, associated with the launching and operation of WIRE. We also thank the referee, T. Bedding, for his careful review of the paper. STF acknowledges the support of the School of Physics and Astronomy at the University of Birmingham.

APPENDIX A: VARIATION OF MAXIMUM POWER SPECTRAL DENSITY

Consider a time series of length T , of a stochastically excited p-mode with mean power P and a lifetime τ . The resulting power spectrum peak can then be modelled according to a Lorentzian function with a linewidth, $\Delta = 1/(\pi\tau)$. Therefore, assuming the modal peak is well resolved in frequency, the maximum power spectral density per bin, H , is given by:

$$H = \frac{2P}{\pi T \Delta}. \quad (\text{A1})$$

Notice that Δ is multiplied by T in order to give the width in terms of the number of bins rather than Hz. This expression can be rewritten in terms of the lifetime τ .

$$H = 2P \left(\frac{\tau}{T} \right). \quad (\text{A2})$$

However, were T to be reduced to such an extent that $T \ll \tau$, the underlying profile would be so narrow as to confine all power within a single bin. In this resulting undersampled regime we have conditions that tend towards an undamped sine wave, where $H \sim P$. Therefore, a full description of H in terms of the other parameters is (Chaplin et al. 2003):

$$H = \begin{cases} 2P(T/\tau) & \text{for } T \gg 2\tau \\ P & \text{for } T \ll 2\tau. \end{cases} \quad (\text{A3})$$

Unfortunately, this does not give an adequate description for H when $T \sim 2\tau$. In order to do this we modify equation A2 slightly to give:

$$H = \frac{2P}{(T/\tau) + 2}, \quad (\text{A4})$$

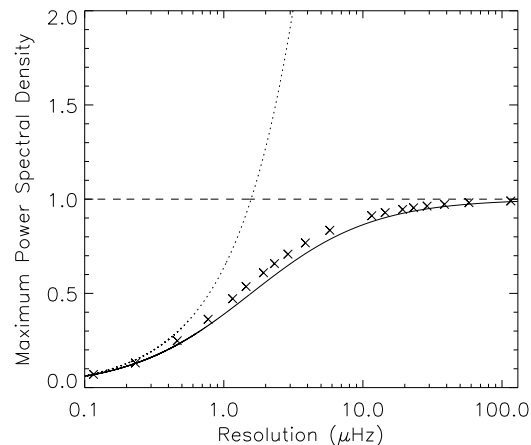


Figure A1. Maximum power spectral density as a fraction of the full modal power determined from the maximum value of 1000 co-added spectra (crosses). We also plot the expected values as determined from the oversampled (dotted line); undersampled (dashed line) and modified (solid line) expressions given in equations A3 and A4.

which can be seen to work in both the over and undersampled regimes.

In order to test equation A4 we produced 1000 artificial time series of a single p-mode signal with linewidth of $1 \mu\text{Hz}$, ranging in length from 100 days down to 0.1 days. The power spectrum of each series was then taken and the independent spectra co-added to produce a smooth peak allowing the maximum power spectral density to be easily measured. In Fig. A1 we compare these values against those predicted from equations A3 and A4. The figure shows clearly how the expressions given in equation A3 diverge away from the true maximum power spectral density in the region $T \sim 2\tau$, whereas equation A4 matches reasonably closely throughout the entire range.

If one wishes to determine the power from the fitted linewidth, Δ and the maximum power spectral density then equation A4 can be rearranged to give:

$$P = H \left(\frac{\pi}{2} T \Delta + 1 \right) \quad (\text{A5})$$

which is the equation used in Section 3.1. We add that even though the results presented in this paper are in the range $T > 2\tau$, we still choose to use this more accurate expression.

REFERENCES

- Bedding, T. R., Kjeldsen, H., Butler, R. P., McCarthy, C., Marcy, G. W., O'Toole, S. J., Tinney, C.G., & Wright, J. T. 2004, *ApJ*, 614, 380
- Bouchy, F., & Carrier, F., 2002, *A&A*, 390, 205
- Buzasi, D. L., Catanzarite, J., Laher, R., Conrow, T., Shupe, D., Gautier III, T. N., Kreidl, T., Everett, D., 2000, *ApJL*, 532, 133
- Chaplin, W. J., Elsworth, Y., Howe, R., Isaak, G. R., McLeod, C. P., Miller, B. A., & New, R., 1997, *MNRAS*, 287, 51
- Chaplin, W. J., Elsworth, Y., Isaak, G. R., Marchenkov, K. I., Miller, B. A., & New, R., 2001, *MNRAS*, 327, 1127

- Chaplin, W. J., Elsworth, Y., Isaak, G. R., Miller, B. A., New, R., Pintér, B., & Thiery, S., 2003, *A&A*, 398, 305
- Fletcher, S. T., Chaplin, W. J., & Elsworth, Y., 2004, in Dansey D., ed, Proc. SOHO 14 / GONG 2004 Workshop (ESA SP-559), Helio- and Asteroseismology: Towards a Golden Future, New Haven, Connecticut, p. 44
- Gizon, L., & Solanki, S. K., 2003, *ApJ*, 589, 1009
- Gabriel, M., Grec, G., Renaud, C., Gabriel, A.H., Robillot, J.M., Roca Cortés, T., Turck-Chièze, S., & Ulrich, R.K., 1998, *A&A* 338, 1109
- Jay, J. E., Guinan, E. F., Morgan, N. D., Messina, & S., Jassour, D., 1996, *AAS*, 29, 730
- Kjeldsen, H., & Bedding, T. R., 1995, *A&A*, 293, 87
- Kjeldsen, H., Bedding, T. R., Butler, R. P., Christensen-Dalsgaard, J., Kiss, L. L., McCarthy, C., Marcy, G. Tinney, C.G., & Wright, J. T. 2005, *ApJ*, in press
- Kuan C-M., 2000, *Intoduction to Economic Theory*, Chapter 4, p. 78
- Morel, P., Provost, J., Lebreton, Y., Thevenin, F., & Berthomieu, G., 2000, *A&A*, 363, 675
- Libbrecht, K. G., 1992, *ApJ*, 387, 712
- Nigam, R. & A. G. Kosovichev, 1998, *ApJ*, 505, L51
- Pourbaix, D., Neuforge-Verheecke C., & Noels, A., 1999, *A&A*, 344, 172
- Saar, S. H, Osten, R. A., 1997, *MNRAS*, 284, 803
- Schou, J., & Buzasi, D. L., 2001, in *Helio- and Asteroseismology at the Dawn of the Millenium*, Proc. SOHO 10/GONG 2000 Workshop, ed. A. Wilson (ESA SP-464: Noordwijk: ESA)
- Toutain, T., & Gouttebroze, P., 1993, *A&A*, 268, 309
- Toutain, T., & Appourchaux, T., 1994, *A&A*, 289, 649
- Walraven, R., 1984, in *Proc. Digital Equipment User's Society*, Anaheim, California